In vivo analysis reveals a critical role for neuropilin-1 in cranial neural crest cell migration in chick

Rebecca McLennan, Paul M. Kulesa *

Stowers Institute for Medical Research, 1000 E. 50th St., Kansas City, MO 64110, USA

Abstract

The neural crest provides an excellent model system to study invasive cell migration, however it is still unclear how molecular mechanisms direct cells to precise targets in a programmed manner. We investigate the role of a potential guidance factor, neuropilin-1, and use functional knockdown assays, tissue transplantation and in vivo confocal time-lapse imaging to analyze changes in chick cranial neural crest cell migratory patterns. When neuropilin-1 function is knocked down in ovo, neural crest cells fail to fully invade the branchial arches, especially the 2nd branchial arch. Time-lapse imaging shows that neuropilin-1 siRNA transfected neural crest cells stop and collapse filopodia at the 2nd branchial arch entrances, but do not die. This phenotype is cell autonomous. To test the influence of population pressure and local environmental cues in driving neural crest cells to the branchial arches, we isochronically transplanted small subpopulations of DiI-labeled neural crest cells into host embryos ablated of neighboring, premigratory neural crest cells. Time-lapse confocal analysis reveals that the transplanted cells migrate in narrow, directed streams. Interestingly, with the reduction of neuropilin-1 function, neural crest cells still form segmental migratory streams, suggesting that initial neural crest cell migration and invasion of the branchial arches are separable processes.
© 2006 Elsevier Inc. All rights reserved.

Keywords: Neuropilin-1; Neural crest; Cranial; Cell migration; Chick; Confocal; Time-lapse imaging

Introduction

The proper assembly of the vertebrate head and peripheral nervous system crucially depends on the emergence and accurate targeting of intrinsically migratory, multipotent cells, called the neural crest. The programmed invasion of the neural crest requires a complex interplay between signals from the neural tube, the surrounding environment and the ability of the cells to properly interpret guidance cues. Defects in any single aspect of this event may translate into craniofacial and cardiac abnormalities and enteric and other autonomic nervous system malformations (Mooney and Siegel, 2002; Farlie et al., 2004; Gershon and Ratcliffe, 2004). Cranial neural crest cells (NCCs) contribute to neurons and glia of the sensory ganglia and to bone, cartilage and pigment cells of the face and neck (Baker and Bronner-Fraser, 1997; Le Douarin and Kalcheim, 1999; Le Douarin et al., 2004). In a striking pattern, cranial NCCs form 3 discrete migratory streams throughout the head, a pattern that is re-capitulated in a wide range of vertebrate systems (Le Douarin and Kalcheim, 1999). The exit points of the streams correlate with specific segmental structures of the hindbrain (Lumsden et al., 1991; Lumsden and Krumlauf, 1996), called rhombomeres. Cranial NCCs from rhombomere 1 (r1), r2 and r3 migrate in a wide stream to populate the 1st branchial arch (Kontges and Lumsden, 1996). NCCs from r3 to r5 sort into a stream that extends lateral to r4 and expands to populate the 2nd branchial arch (ba2). The 3rd branchial arch is composed of NCCs from r5 and r6. Given the complexity of a symphony of cell signaling interactions between the NCCs, the neural tube and the environment, a major question in vertebrate development is how molecular mechanisms consistently produce the stereo-typical cranial NCC migratory pattern.

The combination of tissue transplantation studies, cell tracing and time-lapse analyses in a variety of embryonic systems has contributed to portraying the complexity of NCC migratory behaviors (Bard and Hay, 1975; Newgreen et al., 1979; Tucker and Erickson, 1984; Schilling and Kimmel, 1994;

Kulesa and Fraser, 1998; Halloran and Berndt, 2003; Young et al., 2004). However, it is still unclear how the neural crest interprets intrinsic and environmental signals such that a programmed pattern of invasion emerges. For example, one of the most striking discrete NCC migratory streams extends lateral to r4. Cell labeling studies in chick and mouse show that the cells that emigrate from mid-r3 to mid-r5 contribute to the r4 migratory stream (Sechrist et al., 1993; Birgbauer et al., 1995; Trainor and Krumlauf, 2000). Curiously, the regions adjacent to r3 and r5 remain relatively void of NCCs. It has been suggested that signals within the neural tube may regulate the number of neural crest cells such that r3 and r5 produce fewer NCCs than the even-numbered rhombomeres (Graham et al., 1993, 2004). In contrast, there is strong evidence that environmental signals adjacent to the neural tube play a role in neural crest cell guidance (Trainor and Krumlauf, 2001). Time-lapse studies in chick reveal that a subpopulation of r3 and r5 neural crest cells may migrate into the regions lateral to r3 or r5, but quickly reroute trajectories towards a neighboring stream (Kulesa and Fraser, 1998) and populate the branchial arches. When quail r2 or r4 NCCs are transplanted lateral to r3 in host chick embryos, the cells divert to neighboring streams (Farlie et al., 1999), further suggesting the presence of an inhibitory signal. However, when neural crest cell migratory pathways are blocked by foil barrier transplantation in chick, trailing neural crest cells move around the barriers and re-target towards the branchial arches (Kulesa et al., 2005), suggesting that cell trajectories are not predetermined. Interestingly, chick NCCs can be diverted into the region lateral to r3 when the r3 neuroepithelium and r3 surface ectoderm are ablated (Golding et al., 2002, 2004). Thus, interactions between the emerging NCCs and the local environment play an important role in sculpting and maintaining the discrete NCC migratory streams.

Although several molecular candidates involved in cranial NCC guidance have been identified, the in vivo functional studies are just beginning to emerge (Le Douarin et al., 2004). Previous studies have implicated neuropilin-1 in the migration of both cranial and trunk NCCs from the neural tube to their proper destinations (Eickholt et al., 1999; Osborne et al., 2005). Neuropilin-1, a type 1 membrane protein, is composed of a large extracellular domain and a small cytoplasmic region (reviewed by He et al., 2002; Fujisawa, 2003). Neuropilins act as co-receptors with plexins for secreted forms of semaphorins. Studies suggest that neuropilins bind the corresponding semaphorins and initiate intracellular signaling transduction via plexins (reviewed by Tamagnone and Comoglio, 2000). In 1996, Kawakami and colleagues demonstrated that Neuropilin-1 is expressed by numerous cranial nerves in the murine embryo, including the facial nerve in the 2nd branchial arch (Kawakami et al., 1996). Since then, Neuropilin-1 has been shown to be expressed in discrete tissues of the chick embryo. Specifically, Neuropilin-1 is expressed at the transcript level by migrating cranial NCCs (Eickholt et al., 1999; Gammill and Bronner-Fraser, 2002). Cranial NCCs also express Plexin-A1 transcripts, while semaphorin 3A and semaphorin 3F transcripts are expressed in odd-numbered rhombomeres (Eickholt et al., 1999; Osborne et al., 2005). Interestingly, chick cranial NCCs

avoid substrates containing semaphorin 3A in vitro (Eickholt et al., 1999). These experiments suggest that semaphorin–neuropilin interactions play a role in the initial sculpting cranial NCC streams.

In this paper, we investigate an in vivo role for neuropilin-1 signaling in cranial NCC guidance. To address the in vivo function of neuropilin-1, we use a loss-of-function approach and take advantage of a neuropilin-1 siRNA/EGFP construct (Np-1 siRNA) (Bron et al., 2004) and neuropilin-1–Fc (Np-1–Fc) to perturb endogenous neuropilin-1–ligand interactions. We compare the in vivo migratory patterns of fluorescently labeled Np-1 siRNA transfected and untransfected DiI-labeled cranial NCCs in chick, using 3D confocal microscopy. We analyze the effects of a reduction in neuropilin-1 function on NCC trajectories and cell morphologies using time-lapse confocal imaging. To test the influence of potential inhibitory and permissive cues lateral to the neural tube, we transplant small subgroups of DiI-labeled NCCs isochronically into host embryos ablated of premigratory neighboring neural crest and analyze transplanted cell trajectories over time. We propose a model in which neuropilin-1 is required for cranial NCCs to properly invade specific branchial arches and suggest that multiple, distinct mechanisms shape neural crest cell migratory streams and branchial arch invasion.

Materials and methods

Embryos

Fertilized white leghorn chicken eggs (supplied by Ozark Hatchery, Oeosho, MO, USA) were incubated at 38°C in a humidified incubator until the desired stages of development. Eggs were then rinsed with 70% ethanol and 3 ml of albumin was removed from under the yolk with a 5 ml syringe (309603, Becton Dickinson, Franklin Lakes, NJ, USA) and an 18 gauge needle (305196, Becton Dickinson). A window was cut into the shell and the embryos were visualized by injecting 10% India ink (Pelikan Fount; PLK 51822A143, www.mrart.com, Houston, TX, USA) underneath the area opaca and area pellucida with a 1 ml syringe (309628, Becton Dickinson) and a 25 gauge needle (305112, Becton Dickinson).

Immunohistochemistry

Immunostaining with neuropilin-1 (a kind gift from the Fujisawa laboratory) and HNK-1 was performed on both vibratome sections and whole mount embryos. Both neuropilin-1 (1:100) and HNK-1 (1:20), diluted in 10% goat serum, 4% bovine serum albumen, 0.1% triton-X-100 in phosphate buffered saline (PBS), were incubated with whole mount embryos, hindbrain half preparations or 150 μm vibratome sections overnight at 4°C. After repeated washes, secondary antibodies were applied and incubated at 4°C overnight. The secondary antibodies used for neuropilin-1 and HNK-1 were Alexa Fluor goat anti-rabbit IgG 488 (A-11008, Molecular Probes, Eugene, OR, USA) and Alexa Fluor goat anti-mouse IgM 546 (A-21045, Molecular Probes), respectively.

In ovo electroporation and cell labeling

Embryos were incubated until Stage 9 (Hamburger and Hamilton, 1951), when 6–8 somite pairs were visible. Once an embryo was accessed and visualized, a few drops of sterile Ringer's solution were added over the embryo to prevent it from drying out. A small area of the vitelline membrane above the hindbrain region was removed with a sharpened tungsten needle. Plasmid DNA (5 μg/μl) was injected into the lumen of the neural tube at the axial level of the rostral hindbrain using a pulled borosilicate glass needle (BF100-50-10, Sutter,

Novato, CA, USA) attached to a micromanipulator (M3301, World Precision Instruments, Inc, Sarasota, FL, USA) Picospritzer III (Parker Hannifin Corporation, Fairfield, NJ, USA). We injected plasmid constructs in the form of a control EGFP empty vector named pMES (a kind gift from Cathy Krull, University of Michigan) and siRNA against neuropilin-1 (a kind gift from Frances Lefcort, Montana State University, originally made in the J. Cohen laboratory, MRC Centre for Developmental Neurobiology, London, UK) (Bron et al., 2004). Previous experiments have demonstrated that this construct dramatically knocks down chick neuropilin-1 function in dorsal root ganglia axons (Bron et al., 2004). This vector directs co-expression of both the neuropilin-1 siRNA hairpin and GFP. GFP expression allows for a visual readout of Np-1 siRNA production, but does not delineate neuropilin-1 functional knockdown. In some experiments, a lipophilic dye, DiI (C-7000, Molecular Probes), was mixed with the plasmid DNA and co-injected into the lumen of the neural tube. In tissue transplantation experiments, only DiI was used to fluorescently label premigratory NCCs. For electroporation delivery, on either side of the hindbrain, platinum electrodes were placed parallel to the embryo, 3–5 mm apart. Five pulses of 20 V at 50 ms in duration were applied through the electrodes using an Electro Square Porator ECM 830 (BTX, a division of Genetronics, San Diego, CA, USA). A few more drops of sterile Ringer's solution were applied to the embryo before the egg was resealed with adhesive tape. Eggs were reincubated for 4–36 h, depending on the experiment. After reincubation, embryos were screened for fluorescent labeling and overall health using a fluorescence dissecting microscope (SV11, Carl Zeiss, Thornwood, NY, USA) before being harvested. For static imaging, embryos were fixed in 4% paraformaldehyde for 2 h at room temperature, or 4°C overnight.

Isolation of EGFP positive cells using high purity FACS methodology

Cranial NCCs were electroporated with either pMES or Np-1 siRNA as described. To increase the number of EGFP positive cells, both sides of embryos were electroporated. After 18 h of reincubation, embryos were harvested and membranes removed in cold Ringer's solution. Embryos were prepared into a single cell suspension by treatment with 0.25% Trypsin with EDTA at 37°C for 3 min. This reaction was stopped by addition of fetal bovine serum (FBS) (Invitrogen, Carlsbad, CA). The cells were then centrifuged at 1000 rpm for 5 min and resuspended in PBS with 2% FBS. To visualize viability, the resulting single cell suspension was stained with 2 μg/ml of 7AAD and double sorted using a MoFlo cytometer (Cytomation, Inx, Fort Collins, CO). Equal numbers of EGFP positive and EGFP negative cells were collected from each sample. This resulted in populations of live cells transfected with pMES, Np-1 siRNA, as well as untransfected cells for controls.

RT-PCR analysis of neuropilin-1 expression

We selected RT-PCR to analyze neuropilin-1 expression in cranial NCCs following Np-1 siRNA transfection. The neuropilin-1 antibody was not sensitive enough to detect changes in neuropilin-1 expression in transfected migrating cranial NCCs when the cells are surrounded by untransfected cranial NCCs and unlabeled mesodermal tissue. RNA was isolated from the collected live cells using the RNeasy Mini Kit (74104, Qiagen, Valencia, CA). RT-PCR was then performed using primers for Neuropilin-1 and beta-actin (control). Primers for Neuropilin-1 were 5′-CGGATGGACCCCAGGGGAAG-3′ (forward) and 5′-GCCCAGCCTGAACGGCTTGT-3′ (reverse). Primers for beta-actin were 5′-CGGTTTCGCCGGGGACGATG-3′ (forward) and 5′-CGTCAGGTCACGGC-CAGCCAGA-3′ (reverse). Both resulting DNA products were approximately 500 bp in length. Touchdown PCR was performed using the following conditions: 94°C for 5 min followed by 34 cycles of 94°C for 1 min, annealing temperature decreasing every 2 cycles from 78°C to 62°C for 1 min and 72°C for 1.5 min, then 15 cycles of 94°C for 1 min, 50°C for 1 min and 72°C for 1.5 min. The resulting PCR products were analyzed by gel electrophoresis.

Fc injections

Embryos were incubated until Stage 9 (Hamburger and Hamilton, 1951), and DiI was injected into the lumen of the neural tube as described. Eggs were reincubated for 6 h, at which time r4 cranial NCCs are just starting to emerge from the neural tube. Neuropilin-1–Fc (566-NNS, R&D Systems, Inc) at a concentration of 400 μg/ml was injected into the mesenchyme lateral to r4. The eggs were reincubated for another 18 h, harvested and fixed in 4% paraformaldehyde for 2 h at room temperature, or 4°C overnight.

Tissue transplantations

Embryos were DiI-labeled and in some instances also electroporated with EGFP or Np-1 siRNA at Stages 8–9 (Hamburger and Hamilton, 1951) and reincubated for 1–4 h at 37°C. After reincubation, donor embryos with high levels of fluorescence in the hindbrain were harvested and placed in a Petri dish containing Ringer's solution. From each donor embryo, subregions of the hindbrain (mid-r3 to mid-r5) were removed by making two transverse cuts with a sharpened tungsten needle through the embryo followed by two longitudinal cuts on either side of the neural tube. The dorsal one-third of one side of r4 (region where fluorescently labeled cranial NCCs will delaminate from) was isolated using a glass needle and carefully subdivided transversally into 3–4 tissue pieces. These small subpopulations of r4 NCCs (about 1/6 of the typical size) were individually transplanted into mid-r4 (Stages 8–9) or into the forming ba2 (Stages 15–17) of host embryos, depending on the experiment. Host embryos were unlabeled. Before transplantation, host embryos were prepared differently, depending on the experiment. Some host embryos underwent mid-r3 to mid-r5 ablation; a glass needle was used to remove the dorsal one-third of the neural tube from mid-r3 to mid-r5 (in a similar manner described in Kulesa et al., 2000). This technique was performed at a developmental stage after which no regeneration of cranial NCCs occurs (Sechrist et al., 1995). The ablation removed most but not all of the endogenous cranial NCCs that contribute to the r4 migratory stream. After transplantation, host embryos were either reincubated for 20 h or selected for time-lapse imaging.

Static and time-lapse confocal imaging

After fixation, embryos were washed three times in PBS. Embryonic membranes as well as unnecessary tissues were removed, leaving only the hindbrain intact. The hindbrain was then dissected in half down the midline of the neural tube using a sharpened tungsten needle. This resulted in two hindbrain half preparations that were mirror images of each other. For some immunostaining experiments, 150 μm sagittal vibratome sections of hindbrain regions were cut using a Leica vibratome (VT1000S, Leica, Bannockburn, IL, USA). Hindbrain halves and vibratome sections were prepared for imaging as previously described (Teddy and Kulesa, 2004). For time-lapse confocal imaging, whole embryo cultures were prepared and imaged as previously described (Kulesa and Fraser, 1998).

Quantitative measurements

We analyzed details of the r4 cranial NCC migratory stream using AIM software (Zeiss) to generate 3D volume renderings and 2D projections of confocal image z-stacks. To measure the length of the r4 cranial NCC migratory stream, we defined the lateral edge of r4 as the origin and the distal edge of ba2 as the furthest possible extent of the stream. We used brightfield images to confirm the tissue boundaries. To evaluate the width of the r4 stream, we measured the widths at two distinct locations. First, the thinnest portion of the stream was defined as the width of the stream perpendicular to the center of the otic vesicle. The widest portion of the stream was defined as where the stream was the widest within ba2. To evaluate the 2D area covered by cranial NCCs within ba2, we calculated the mean fluorescence intensity measured within a region of interest drawn around the 2nd branchial arch regions in projected confocal z-stacks. We also measured the average number of filopodial extensions per cell for cells within the 2nd branchial arch and midstream. To calculate the average number of filopodia per cell, 10 cells in each region of interest were selected for study based on their quality of resolution. Regions of interest were defined by drawing rectangles near the thinnest width of the stream

and within the 2nd branchial arch. Statistical analyses were performed using standard Student's *t* test.

Cell death assay (TUNEL)

For detection of cell death, electroporated embryos were harvested, fixed and cleaned as described above. The protocol within the In Situ Cell Death Detection Kit, TMR red (2156792, Roche, Indianapolis, IN, USA) was followed. Cell death was analyzed using 543 nm excitation to visualize TMR fluorescence within cells of the r4 cranial NCC migratory stream in embryos using confocal microscopy (LSM5 Pascal, Zeiss).

Results

We investigated the cellular and molecular mechanisms underlying the sculpting of cranial NCC migratory streams. We focused our in vivo analyses to the NCC migratory stream that emerges lateral to r4 as a model for NCC migratory stream formation. Previous cell lineage tracing has shown that the cranial NCC stream emerging lateral to r4 is composed of cranial NCCs that arise from mid-r3 to mid-r5. For simplicity, we define the NCC migratory stream that emerges adjacent to r4 as the r4 cranial NCC migratory stream.

Neuropilin-1 protein is expressed by cranial NCCs in the r4 migratory stream

Previous studies examining the expression of neuropilins in the developing vertebrate embryo have focused at the transcript level. We asked whether or not Neuropilin-1 is expressed by NCCs at the protein level. We found that cranial NCCs expressed Neuropilin-1 along the length of the typical migratory pathways (Fig. 1). Longitudinal (Figs. 1A–H) and transverse (Figs. 1I–L) sections showed that cranial NCCs within the r4 and r6 migratory streams expressed Neuropilin-1. This expression correlated with HNK-1, a typical membrane marker for avian NCCs (Figs. 1A–L). Interestingly, Neuropilin-1 expression was also detected in r4, which was not previously identified via in situ hybridization. This may be due to differences between transcript and protein signals detected, or differences in the age of the embryos examined.

Np-1 siRNA reduces expression of neuropilin-1 in vivo

To test the effectiveness of the Np-1 siRNA construct in vivo, we performed RNA isolation followed by RT-PCR on a
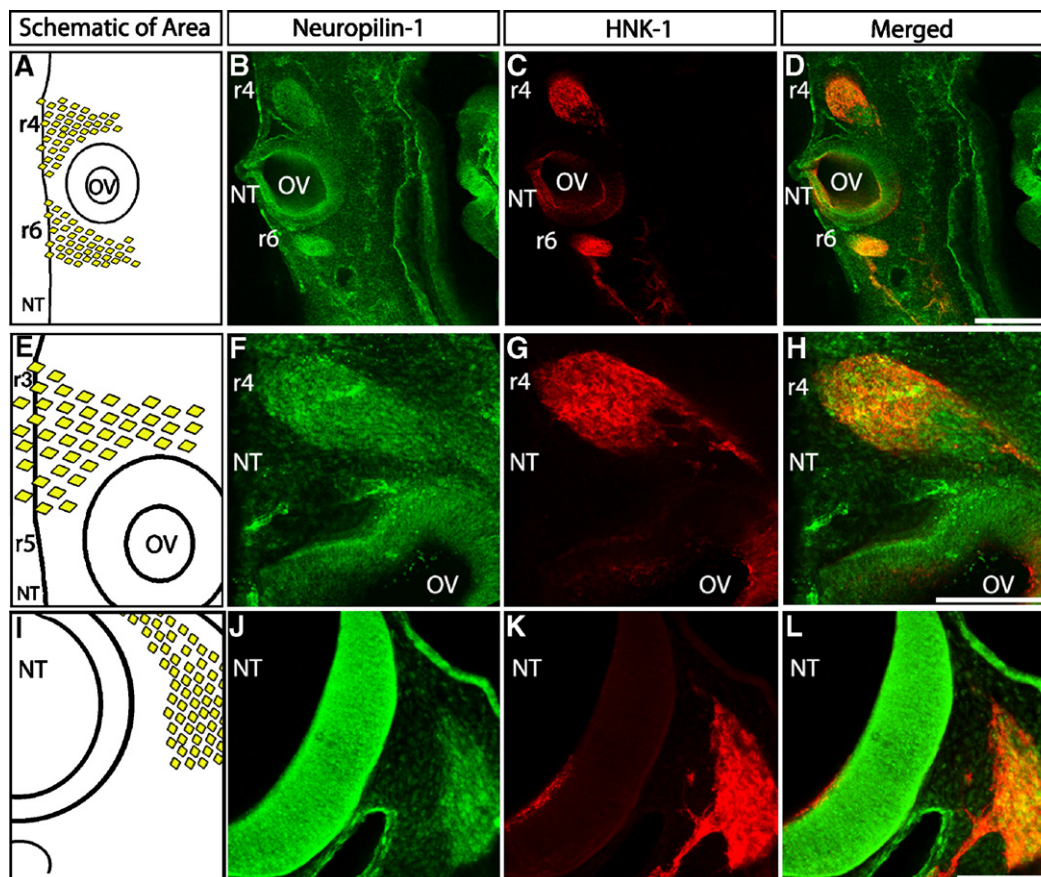

Fig. 1. Neuropilin-1 protein is expressed by migrating r4 cranial NCCs. (A, E, I) Schematic representations of sections through chick embryos. (A) Coronal (longitudinal) section through the hindbrain, showing both the r4 and r6 NCC migratory streams and otic vesicle (OV) and neural tube (NT). (B–D) The same coronal section as depicted in (A) showing the neuropilin-1 antibody (green) and HNK-1 antibody (NCC marker-red) and overlaid images (merged) in a Stage 16 embryo. The otic vesicle is approximately 100 μm in diameter. (F–H) A closer view of the staining pattern of a typical Stage 16 chick embryo showing the r4 NCC migratory stream. (J–L) Transverse section through a typical Stage 16 embryo at the r4 level, stained. Neuropilin-1 expression was localized to migratory cranial NCCs. The scale bars are 100 μm in D, H and L. The notations are r, rhombomere, ba, branchial arch, OV, otic vesicle, NT, neural tube.

reasonably pure population of GFP positive cells. These cells were obtained via FACS on cells disassociated from electroporated embryos. We used primers specific for chick neuropilin-1 and beta-actin (internal control). The results indicate that, in Np-1 siRNA transfected cells, neuropilin-1 expression is greatly reduced when compared to neuropilin-1 expression in cells transfected with EGFP control (Fig. 2I).

Cranial NCCs fail to completely invade the branchial arches when Np-1 function is disrupted

To test the in vivo function of neuropilin-1 in NCC guidance, we used in ovo electroporation to target chick Np-1 siRNA (Bron et al., 2004) into premigratory cranial NCCs. Analysis of static confocal 3D image z-stacks revealed dramatic differences in the distribution of cranial NCCs in the distal portions of their migratory pathway. We found that cranial NCCs transfected with Np-1 siRNA failed to completely invade the branchial arches (compare Fig. 2B with A). When focusing on the r4 stream, cranial NCCs did not migrate to distal portions of ba2 and did not spread out to cover the anterior–posterior width of the branchial arch (Figs. 2D and E). Interestingly, cranial NCCs transfected with Np-1 siRNA did not invade regions lateral to r3 and r5 (Figs. 2B and E), consistent with the control scenario (Fig. 2A). Along the proximo-distal length of the r4 cranial NCC migratory stream, both Np-1 siRNA and control scenarios exhibited similar
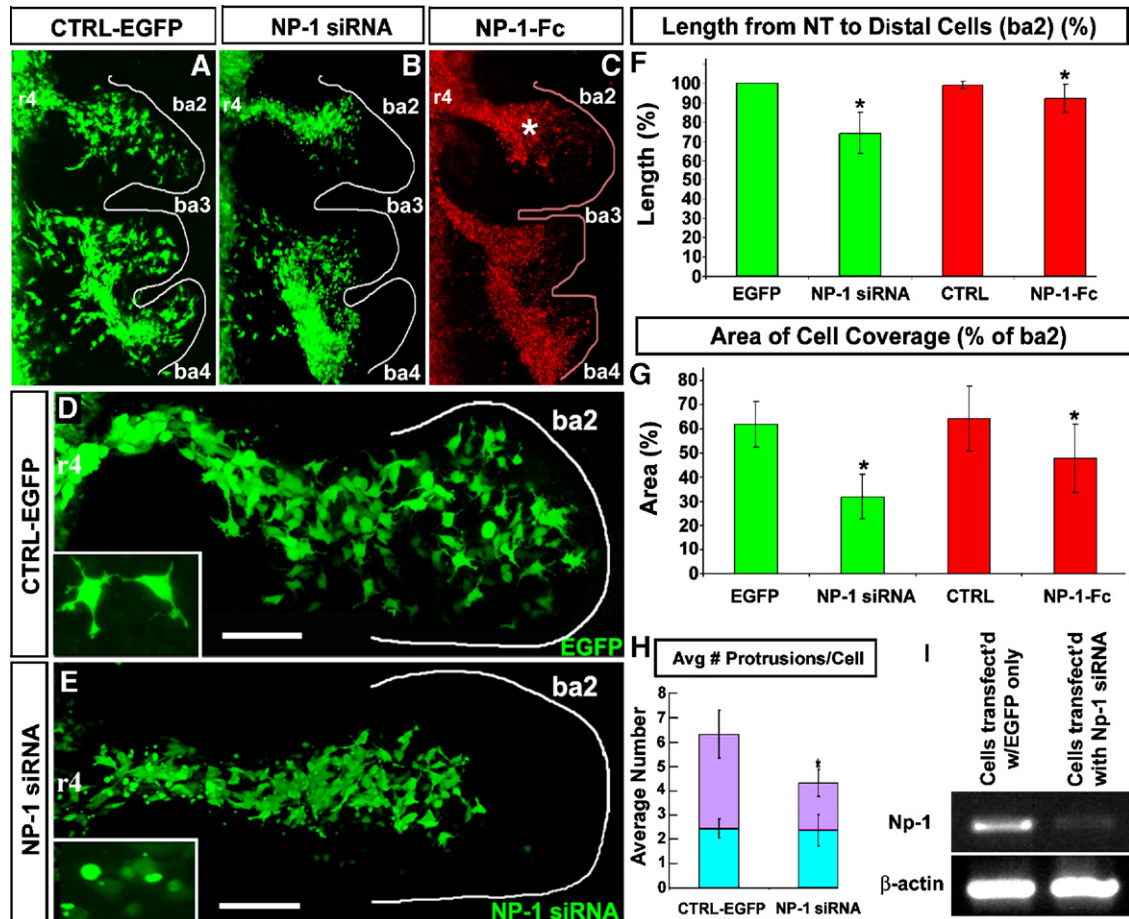

Fig. 2. Cranial NCCs fail to completely invade the 2nd branchial arch when neuropilin-1 function is knocked down. (A) Static confocal image of a typical embryo in which cranial NCCs were transfected with a control EGFP construct, $n=7$. The transfected cranial NCCs migrated normally from the neural tube and populated the branchial arches. (B) Static confocal image of an embryo in which cranial NCCs were transfected with Np-1 siRNA, $n=11$. The Np-1 siRNA transfected cells were able to migrate out of the neural tube in a typical pattern, however the cells failed to completely invade the branchial arches. (C) Static confocal image of a DiI-labeled embryo in which Np-1–Fc was injected into the pathway of r4 cranial NCCs, $n=11$. (D) Static confocal image of the r4 cranial NCC stream in which cranial NCCs were transfected with a control EGFP construct, $n=7$. The transfected cranial NCCs migrated normally from the neural tube, forming a condensed stream and then spread out to populate the entire area of ba2. Inset shows cells in ba2, with many filopodial protrusions. (E) Static confocal image of the r4 cranial NCC stream in which cranial NCCs were transfected with Np-1 siRNA, $n=11$. The Np-1 siRNA transfected cells were able to migrate out of the neural tube and form the r4 stream, however the cells failed to completely invade ba2. The inset shows cells in ba2, with a rounded-up phenotype. (F) Quantitative measurements of the distance cranial NCCs migrated from the neural tube into ba2, as a percentage of the distance from the neural tube to the distal end of ba2 (100%). (G) Quantitative measurements of the mean fluorescence intensity of EGFP in the area of ba2. (H) Quantitative measurements of the average number of filopodial protrusions per cell in the r4 midstream (blue bars) and in ba2 (purple bars). (I) RT-PCR demonstrated that, when cells were transfected with Np-1 siRNA, the expression levels of neuropilin-1 were reduced. The scale bars are 50 μm in D and E. The notations are r, rhombomere, ba, branchial arch, OV, otic vesicle, *, significantly different, $p=0.000$ for length from NT to distal cells, comparing Np-1 siRNA transfected cells to EGFP only transfected cells, $p=0.005$ for length from NT to distal cells, comparing Np-1–Fc injected side to control side, $p=0.000$ for area of cell coverage, comparing Np-1 transfected cells to EGFP only transfected cells, $p=0.012$ for area of cell coverage, comparing Np-1–Fc injected side to control side, $p=0.000$ for average number of protrusions per cell in ba2, comparing Np-1 transfected cells to EGFP only transfected cells.

shapes at midstream (compare Fig. 2D with E). To determine whether the midstream characteristics of the r4 NCC stream were affected in Np-1 siRNA transfected embryos, we measured the midstream widths. We found that the width of the midstream in embryos transfected with Np-1 siRNA (54.1 μm±7.1 μm) was not significantly different when compared with that of control embryos (50.9 μm±14.1 μm). We also measured the distance from the neural tube to the point where the cranial NCC stream spreads out in a fan-like pattern at the entrance to the 2nd branchial arch. When cranial NCCs were transfected with Np-1 siRNA, the distance from the neural tube to the start of the spread (40.3%±7.8% of the distance from the neural tube to the distal end of ba2) was not significantly different when compared to this distance for cranial NCCs transfected with the control construct (40.7%± 3.6% of the distance from the neural tube to the distal end of ba2). Therefore, the morphology of the r4 cranial NCC stream near the neural tube was statistically equivalent when transfected with Np-1 siRNA or a control EGFP construct.

In contrast, when we compared the branchial arch invasion of NCCs transfected with Np-1 siRNA construct to that of cells transfected with a control EGFP construct, Np-1 siRNA transfected cells only migrated 74.1% (±10.6%) of the distance from the neural tube to the distal end of ba2 (Fig. 2F). Similarly, near the entrance to ba2, cranial NCCs only spread out into the branchial arch 70.2% (±16.1%) of the arch width. When cranial NCCs were transfected with a control EGFP construct, 62% (±9.5%) of the 2nd branchial arch area contained transfected cranial NCCs (Fig. 2G). However, when cells were transfected with Np-1 siRNA, the area of coverage was significantly reduced, with only 31.9% (±9.2%) of ba2 containing transfected cranial NCCs (Fig. 2G).

To confirm the effect of knocking down neuropilin-1 signaling, we injected Np-1–Fc into the mesenchyme lateral to r4 at a time shortly after r4 cranial NCCs emerged from the neural tube. The Np-1–Fc will bind to neuropilin-1 ligands, preventing any endogenous neuropilin-1 from binding to those ligands, hence knocking down endogenous neuropilin-1 signaling. Cranial NCCs failed to migrate completely into ba2 when the migratory pathway contained Np-1–Fc (Fig. 2C). The NCC migration was normal on the uninjected side of the embryo (Figs. 2F and G). When the migratory pathway contained Np-1–Fc, r4 cranial NCCs migrated 92.1% (±7.3%) of the distance possible (Fig. 2F). When DiI-labeled cranial NCCs were not exposed to Np-1–Fc, 64.3% (±13.6%) of the 2nd branchial arch contained DiI signal (Fig. 2G). In comparison, when DiI-labeled cranial NCCs were exposed to Np-1–Fc, 48% (±14.2%) of the 2nd branchial arch contained DiI signal (Fig. 2G).

Cranial NCC transfected with Np-1 siRNA display rounded cell morphologies, but no increase in cell death near the branchial arch entrances

The r4 cranial NCCs transfected with Np-1 siRNA appeared to be more rounded in shape than cells transfected

with a control EGFP construct, near the branchial arch entrance (compare Fig. 2E inset with D inset). Cells within the midstream of a typical r4 cranial NCC migratory stream had an average of 2.4 (±0.4 and ±0.6) filopodia when transfected with a control EGFP construct or Np-1 siRNA (Fig. 2H, blue). However, knocking down neuropilin-1 function significantly reduced the average number of filopodia per cell from 6.3 (±1.0) filopodia to 4.3 (±0.6) filopodia near the entrance to the 2nd branchial arch (Fig. 2H, purple). TUNEL analysis showed that the cells transfected with Np-1 siRNA did not undergo premature cell death (data not shown).

The phenotype caused by functional knockdown of neuropilin-1 is cell autonomous

To investigate whether the neuropilin-1 knockdown phenotype was cell autonomous, or whether surrounding, untransfected NCCs were also affected, we co-injected the DNA plasmid constructs with DiI. Using this method, we could visualize nearly all untransfected cells (DiI-labeled) and transfected cells (EGFP/DiI-labeled). When cranial NCCs were transfected with a control construct, the transfected (Fig. 3A, green) and untransfected (Fig. 3A, red) cranial NCCs completely invaded the entire region of ba2. In the Np-1 siRNA electroporated embryos, transfected cells failed to spread out into the 2nd branchial arch (Fig. 3B, green), however DiI-labeled cells completely invaded ba2 (Fig. 3B, red). Sagittal sections through the 2nd branchial arch (Figs. 3A and B; dotted lines) showed the dramatic difference between the invasion of control and Np-1 siRNA transfected cranial NCCs (compare Fig. 3D with C). Specifically, the Np-1 siRNA transfected cells did not spread into the anterior and posterior regions of the 2nd branchial arch (Fig. 3D). Quantitative measurements showed that Np-1 siRNA transfected cells reach only 77.9% (±12.1%) of the distance to the distal end of ba2 (Fig. 3E) and spread out 69.7% (±15.5%) of the width of ba2 (Fig. 3F). However, the distances that DiI-labeled cells migrated in embryos electroporated with Np-1 siRNA or with a control EGFP construct were statistically equivalent (Figs. 3E and F).

To confirm that our observed phenotype was not due to a delay in Np-1 siRNA production, we transplanted dorsal r4 subregions from donor embryos that were electroporated with Np-1 siRNA and reincubated for 4–6 h before transplantation. After 4–6 h of incubation, tissue from the r4 region in the donor embryos was visualized for GFP fluorescence to confirm activation of Np-1 siRNA expression prior to transplantation into mid-r4 of host embryos and migration. In host embryos, thin streams containing both DiI and EGFP labeling formed adjacent to r4, however the Np-1 siRNA transfected cells failed to migrate as far as the DiI-labeled cells (Fig. S1-H). This situation mimicked the phenotype observed when r4 cranial NCCs were electroporated with Np-1 siRNA and did not undergo transplantation procedures (Fig. 2E).

Cranial NCCs transfected with Np-1 siRNA intermingle with other untransfected NCCs, but stop and collapse filopodia near the entrance to the 2nd branchial arch

To examine the in vivo function of neuropilin-1 on cranial NCC migratory behaviors, we followed individual fluorescently labeled cranial NCCs in whole chick embryos. Time-lapse confocal imaging revealed that, when cranial NCCs were transfected with a control EGFP construct and labeled with DiI, EGFP positive cells (Fig. 4, left column, green cells) were seen throughout the DiI-labeled migratory stream (Fig. 4, left column, red cells; see Movie 1). Importantly, EGFP cells mixed with DiI-labeled NCCs throughout a typical r4 NCC migratory stream, including the front of the stream (Fig. 4, left column, arrowhead). Cranial NCCs transfected with Np-1 siRNA behaved noticeably different from control NCCs in two ways. First, Np-1 siRNA transfected cranial NCCs (Fig. 4, right column, green cells) emerged later than the untransfected DiI-labeled cells (Fig. 4, right column, red cells; see Movie 2). In a typical transfected embryo, the front of the r4 migratory stream was comprised of only DiI positive cells (Fig. 4, right column, asterisk). Np-1 siRNA cells lagged behind the stream front (Fig. 4, right column, arrow). Second, when Np-1 siRNA transfected cranial NCCs reached the entrance of ba2, the cells stopped and collapsed filopodia (Fig. 4, right column, compare the cell shape (arrow) at $t=1$ h with $t=2.5$ h and $t=4.2$ h; see Movie 2). DiI-positive cells were able to migrate further than Np-1 siRNA transfected cells and spread into the 2nd branchial arch (Fig. 4, right column, blue and yellow circled cells; see Movie 2).

To test whether the Np-1 siRNA r4 cranial NCC phenotype was due to the environment or timing of downstream signaling cascades in the cells, tissue containing Np-1 siRNA or control tissue (EGFP only transfected) and DiI-labeled premigratory r4 cranial NCCs were transplanted directly into ba2 of Stages 15–17 (Hamburger and Hamilton, 1951) embryos. In embryos receiving transplants electroporated with Np-1 siRNA, DiI-labeled cells migrated to invade ba2, but Np-1 siRNA positive cells remained in or near the transplant site (Figs. S1-D and E).
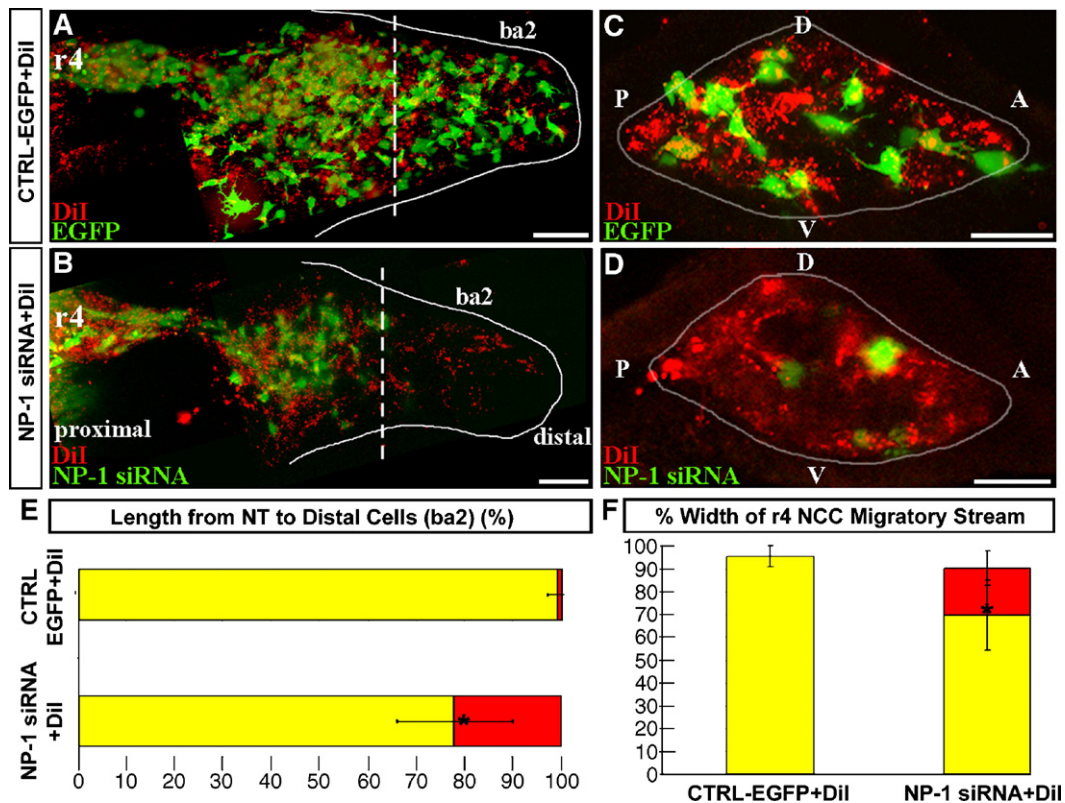

Fig. 3. The neuropilin-1 function in cranial NCCs is cell autonomous. Some cranial NCCs were transfected with EGFP construct of interest (green), while the majority of cranial NCCs were labeled with DiI (red). (A) A static confocal image shows that, when cranial NCCs were transfected with EGFP only, the transfected (green) and untransfected (red) cells migrated from the neural tube and invaded the entire region of ba2, $n=6$. The dashed line indicates the position of cross-section cut. (B) Static confocal image showing that, when cranial NCCs were transfected with Np-1 siRNA, the transfected cells (green) were unable to invade ba2, unlike the untransfected cells (red), $n=9$. The dashed line indicates the position of a cross-section cut. (C) Static confocal image of a sagittal section through ba2 after cranial NCCs were transfected with EGFP only and labeled with DiI. Transfected cells were observed throughout ba2. (D) Static confocal image of a typical sagittal section through ba2 after cranial NCCs were transfected with Np-1 siRNA and labeled with DiI. Transfected cells were unable to appropriately enter ba2, unlike untransfected cells. (E) Quantitative measurements of the distance cranial NCCs migrated from the neural tube into ba2, as a percentage of the distance from the neural tube to the distal end of ba2. (F) Quantitative measurements of the anterior–posterior width cranial NCCs spread out in ba2 as a percentage of the total width of ba2. The scale bars are 50 μm in A–D. The notations are r, rhombomere, ba, branchial arch, P, posterior, A, anterior, D, dorsal, V, ventral, *, significantly different, $p=0.001$ for length from NT to distal cells, comparing Np-1 siRNA transfected cells to EGFP only transfected cells, $p=0.002$ for width of r4 NCC migratory stream, comparing Np-1 transfected cells to EGFP only transfected cells.

develop for an additional 12 h (for a total of 36 h after electroporation). In a typical chick embryo, by this developmental stage, both control EGFP transfected (Fig. 5A, green) and DiI-labeled (Fig. 5A, red) cranial NCCs have completely
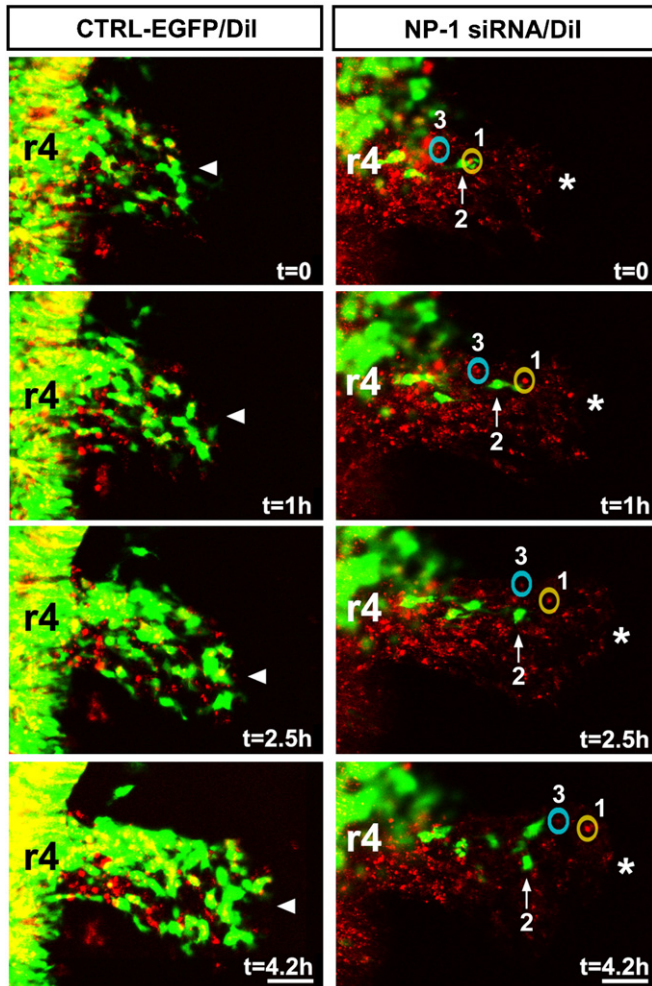

Fig. 4. Transfected cells exhibited delayed migration and prematurely stop when neuropilin-1 function in migrating r4 cranial NCCs is knocked down. Selected images from a typical time-lapse imaging session show cranial NCCs migrating in the r4 cranial NCC stream. The majority of cranial NCCs were labeled with DiI (red), while some were transfected with either EGPF control (green, left column) or Np-1 siRNA (green, right column). (Left column) EGPF positive cells were spread throughout the migratory stream and were at the leading edge with the DiI positive cells (arrowhead). (Right column) DiI-labeled cells were seen at the leading edge of the stream (asterisk). Np-1 siRNA transfected cells (an example of a cell is shown by the arrow) lagged behind the leading edge of the migratory stream (asterisk) and then prematurely stopped ($t=2.5$ h, arrow). The lead transfected cell did not move very much from $t=2.5$ h to $t=4.2$ h. DiI-labeled untransfected cells were able to migrate further (yellow circled cell, 1) than Np-1 siRNA transfected cells and continued to migrate past the Np-1 siRNA transfected cells (2) and into the 2nd branchial arch (blue circled cell, 3). The scale bars are 50 μm. The notation is r, rhombomere.

When the transplanted tissue contained EGFP transfected and DiI-labeled cells, cells migrated randomly from the transplant site (Figs. S1-B and C).

Cranial NCCs transfected with Np-1 siRNA do not completely invade the 2nd branchial arch at later stages of development

To examine whether the failure of Np-1 siRNA transfected NCCs to completely invade the 2nd branchial arch was due to a delay in migration, we allowed electroporated embryos to
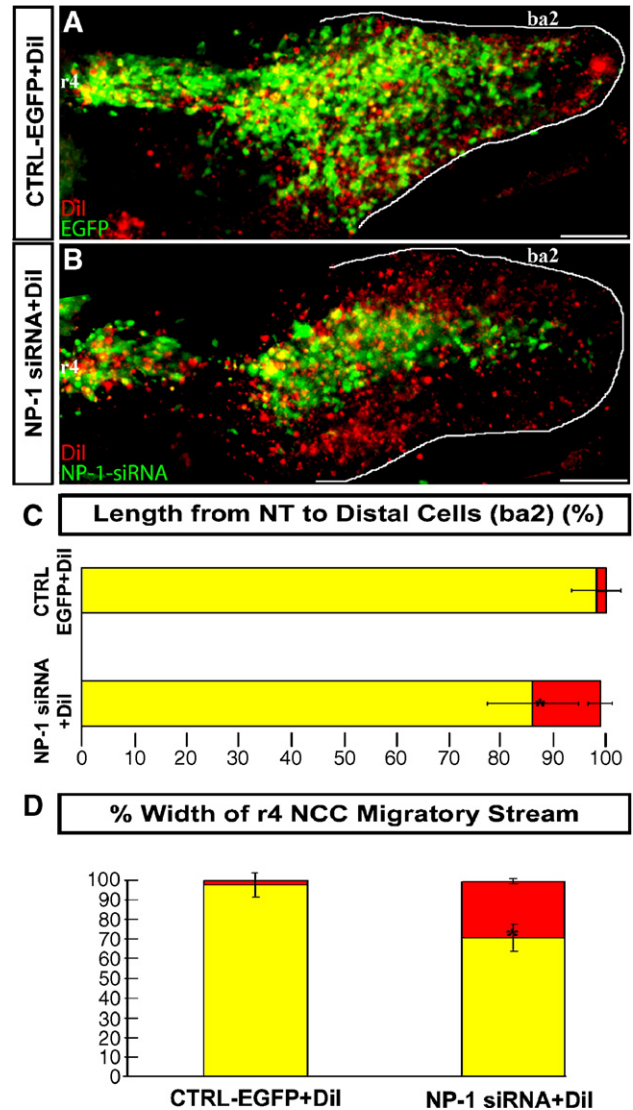

Fig. 5. When neuropilin-1 function in migrating r4 cranial NCCs is knocked down, the phenotype does not recover at later developmental stages. Some cranial NCCs were transfected with EGFP construct of interest (green), while the majority of cranial NCCs were labeled with DiI (red). (A) A static confocal image of a typical embryo when cranial NCCs were transfected with EGFP only, the transfected (green) and untransfected (red) cells migrated from the neural tube and invaded the entire region of ba2, $n=12$. (B) Static confocal image shows that, when cranial NCCs were transfected with Np-1 siRNA, the transfected cells (green) were unable to migrate throughout ba2, unlike the untransfected cells (red), $n=12$. (C) Quantitative measurements of the distance cranial NCCs migrated from the neural tube into ba2, as a percentage of the distance from the neural tube to the distal end of ba2. (D) Quantitative measurements of the width cranial NCCs spread out in ba2 as a percentage of the total width of ba2. The scale bars are 100 μm in A and B. The notations are r, rhombomere, ba, branchial arch, *, significantly different, $p=0.006$ for length from NT to distal cells, comparing Np-1 siRNA transfected cells to EGFP only transfected cells, $p=0.000$ for width of r4 NCC migratory stream, comparing Np-1 transfected cells to EGFP only transfected cells.

invaded ba2. In contrast, Np-1 siRNA transfected cranial NCCs still did not fully invade the branchial arch (compare Fig. 5B and A), although some cells were able to migrate further towards the distal portion of ba2. The Np-1 siRNA transfected cells failed to invade the anterior and posterior regions of ba2 (Fig. 5B) and maintained a dense cohort of cells. Quantitative measurements confirmed that the Np-1 siRNA transfected cells reach only 86.1% (±8.6%) of the proximo-distal distance from the neural tube to the distal portion of the 2nd branchial arch (Fig. 5C) and 70.8% (±6.9%) of the width of the migratory stream (Fig. 5D).

Subpopulations of r4 cranial NCCs transplanted into mid-r4 of host embryos migrate in narrow, directed streams to the 2nd branchial arch

Many hypotheses of NCC stream formation have suggested that migratory streams are sculpted from population pressure and local environmental inhibitory cues. Mechanistically, NCCs that initially emerge from the neural tube and enter the lateral environment are thought to be pushed from behind by the constant source of NCCs at the neural tube midline. Local environmental cues, in the form of repulsive cues lateral to r3 and r5 and permissive cues adjacent to r4, may sculpt the NCCs into a dense migratory stream. To address these hypotheses, we first asked whether decreasing the number of cranial NCCs exiting from r4 leads to a stream formation. That is, without significant pressure from behind, do NCCs emerging lateral to r4 stop or continue to migrate to the 2nd branchial arch? Second, do cranial NCCs emerging from r4 require contact with inhibitory regions lateral to r3 and r5 to reach peripheral locations?

To approach these questions, we transplanted small subgroups of DiI-labeled premigratory r4 cranial NCCs into the mid-r4 region of host embryos of the same developmental stage (Fig. 6A). Prior to the donor transplantations, we ablated many
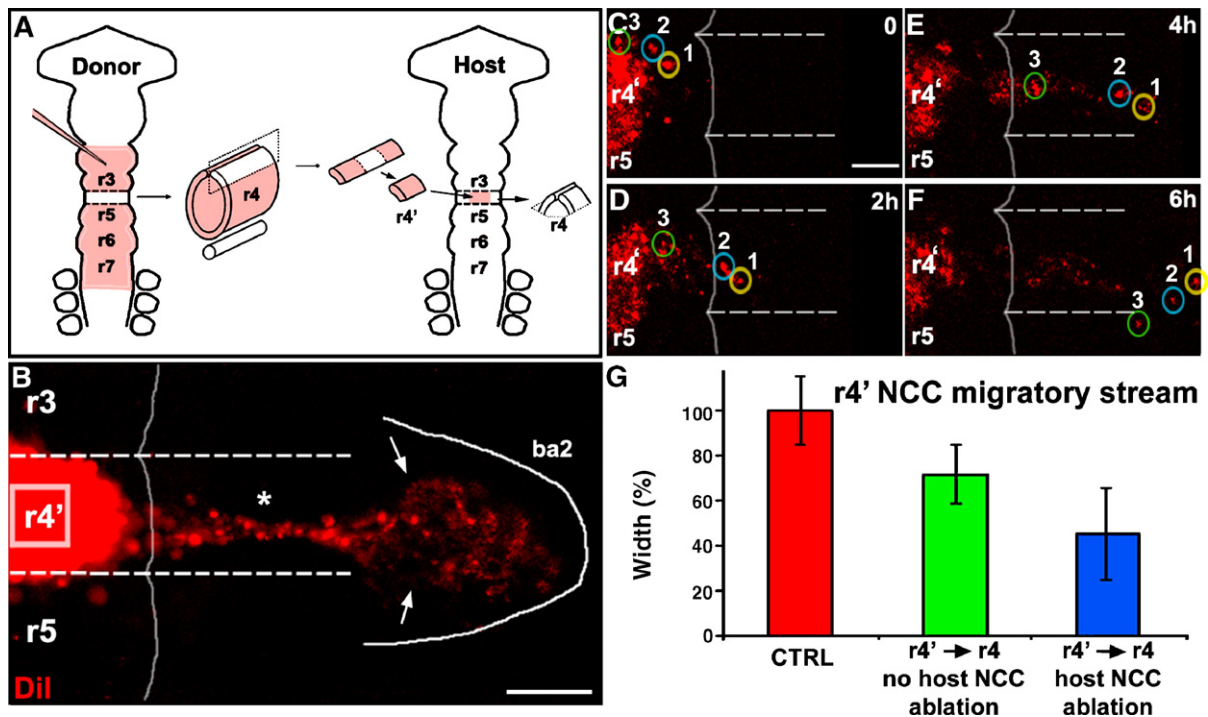

Fig. 6. Transplantation studies reveal that subpopulations of donor r4 cranial NCCs migrate towards the 2nd branchial arch from the r4 region of host embryos in a highly directed manner. (A) A schematic representation of transplantation technique. A typical donor embryo was injected with DiI at Stages 8–9 (needle and red color) and reincubated for 4 h. The r4 region was removed and the right-hand side of dorsal r4 was cut into 3–4 pieces. The host embryo was either untreated, injected with DiI, or underwent a mid-r3 to mid-r5 ablation (as depicted). (B) A static confocal image of a typical host embryo, 20 h after a subpopulation of DiI-labeled r4 NCCs (red) were transplanted into the r4 region of a host embryo with mid-r3 to mid-r5 ablation of one-third of the neural tube. An r4′ marked in a box designates the original size of the transplanted r4 cells before the image was overexposed to show the narrow stream of migrating cells. The DiI-labeled transplanted cells migrated out from r4 in a narrow stream (asterisk) and did not migrate into the regions lateral to r3 and r5 (marked by the horizontal dashed lines). Upon reaching the entrance to ba2, the transplanted cranial NCCs spread throughout the branchial arch (arrow). (C, D, E, F) Selected images from a typical time-lapse imaging session show transplanted cranial NCCs (DiI-labeled in red) forming a narrow stream from r4. (C) Time-lapse imaging started 4 h after the transplantation experiment. DiI-labeled cells were starting to emigrate from the neural tube (yellow-, green- and blue-circled cells). (D) At *t*=2 h (h), DiI-labeled cells emigrated past the outline of the neural tube (faint gray line) and formed a narrow stream (yellow- and blue-circled cells). (E) At *t*=4 h, all the circled cells moved further lateral and did not meander through the presumptive permissive corridor. (F) At *t*=6 h, upon reaching ba2, DiI-labeled cells spread out into ba2 (yellow-, green- and blue-circled cells). (G) Quantitative analysis showed the width of the migratory streams after different manipulations. For the control (red bar; *n*=14), untreated embryos were labeled with DiI and the resulting widths of the r4 NCC midstreams were measured. DiI-labeled r4 cells were transplanted into hosts that either underwent a mid-r3 to mid-r5 dorsal one-third ablation (blue bar; *n*=21) or no ablation (green bar; *n*=10). All of the experimental manipulations resulted in midstream widths that were significantly different to the control width, *p*=0.00 (green bar compared with red bar), *p*=0.00 (blue bar compared with red bar). The scale bars are 50 μm in B and C. The notations are r, rhombomere, ba, branchial arch.

of the premigratory NCCs from mid-r3 to mid-r5 in host embryos. Static confocal analyses revealed that the DiI-labeled transplanted r4 NCCs formed a migratory stream and reached the 2nd branchial arch (Fig. 6B). The shape of the NCC migratory stream formed by transplanted cells was narrow from the neural tube to the entrance to ba2 (Fig. 6B, asterisk). Near the entrance to ba2, the migratory stream widened and dramatically spread out into ba2 (Fig. 6B, arrows). Time-lapse confocal analyses revealed that transplanted r4 cranial NCCs emerged from the neural tube and migrated in a directed manner towards ba2, without contacting regions lateral to r3 or r5 (Figs. 6C–F; see Movie 3). Only a few individual DiI-labeled NCCs were observed to leave a stream and migrate towards the regions lateral to r3 and r5, but most of these cells returned to the r4 stream (data not shown). Individual transplanted cells formed into and maintained a narrow stream of cells to the entrance of ba2 (Figs. 6C–E, yellow, green and blue circles). After arriving at the ba2 entrance, the cells dispersed widely to spread out into ba2 (Fig. 6F, yellow, green and blue circles). Measurements of the migratory stream formed from transplanted NCCs showed that the average midstream width was only 45.2% (±20.6%) of a typical control r4 NCC migratory stream (Fig. 6G, red versus blue). In comparison, the average midstream width of an r4 cranial NCC migratory stream comprised of NCCs transplanted into a non-ablated host embryo was 71.6% (±13.0%) of the control (Fig. 6G, red versus green).

Discussion

In this study, we presented in vivo evidence that neuropilin-1 signaling mediates the invasion of cranial NCCs into the branchial arches. We analyzed in vivo changes in NCC migratory behaviors, cell morphologies and migratory stream formation in an embryonic chick system, using tissue transplantations, molecular perturbations and confocal time-lapse imaging. We showed that cranial NCCs transfected with Np-1 siRNA failed to fully invade the branchial arches. Injections of Np-1–Fc along the NCC migratory routes, ahead of emerging NCC streams, showed a similar affect. This phenotype was not as striking as the Np-1 siRNA phenotype, which may been due to dilution of the Np-1–Fc solution at the injection site. The Np-1 siRNA phenotype was cell autonomous and especially striking at the 2nd branchial arch. Time-lapse confocal imaging revealed that Np-1 siRNA transfected cranial NCCs altered cell migratory behaviors and cell morphologies near the 2nd branchial arch entrance. However, transfected NCCs properly sorted into and formed typical migratory streams. To test whether population pressure and local inhibitory cues shape the initial formation of cranial NCC migratory streams, we isochronically transplanted small sub-populations of DiI-labeled r4 NCCs into r4 of host embryos ablated of premigratory mid-r3 to mid-r5 NCCs. Interestingly, transplanted NCCs migrated in narrow, directed streams to ba2, without sampling regions adjacent to r3 or r5. Our results demonstrate an in vivo role for neuropilin-1 signaling to mediate NCC branchial arch invasion and suggest that multiple mechanisms sculpt migratory stream shape and maintenance.

Neuropilin-1 siRNA transfected cranial NCCs properly sort into discrete migratory streams but fail to invade the branchial arches, suggesting neuropilin-1 functions to promote full invasion of NCC into specific target sites. Our results are consistent with the idea that neuropilin–semaphorin interactions mediate NCC invasion of peripheral targets (Feiner et al., 2001). In semaphorin 3C mutant mice, NCC migration from the branchial arches into the cardiac outflow tract is impaired (Feiner et al., 2001). Semaphorin 3C is expressed in the developing outflow tract at a time consistent with the migration of cardiac NCCs into the outflow tract (Feiner et al., 2001). Interestingly, in our results and in semaphorin 3C mutant mice, NCCs properly reach the branchial arches suggesting that different neuropilin–semaphorin interactions may mediate separate NCC migratory events. We were surprised that the knockdown of neuropilin-1 gave such a dramatic phenotype focused on the 2nd branchial arch. However, the knockdown of Fgfr1 signaling in mice (Trokovic et al., 2003), a singular perturbation, also independently leads to a significant loss of neural crest cells within the 2nd branchial arch region. Thus, the proper entry of cranial NCCs into the 2nd branchial arch may require the simultaneous interactions of multiple components.

Cranial NCCs form typical, discrete migratory streams in neuropilin-1 perturbed embryos, suggesting that the initial segmental NCC migration pattern may not crucially depend on neuropilin-1 signaling. A priori, we did not expect that Np-1 siRNA transfected cranial NCCs would respect NCC exclusion zones lateral to r3 and r5 (Farlie et al., 1999). Previous data in chick and zebrafish have suggested that neuropilin–semaphorin interactions sculpt cranial NCCs into discrete migratory streams (Eickholt et al., 1999; Yu and Moens, 2005; Osborne et al., 2005). Chick cranial NCCs exposed in vitro to semaphorin 3A–Fc (semaphorin 3A is expressed in r3 and r5) displayed rounded-up cell morphologies and avoided semaphorin 3A–Fc-rich regions (Eickholt et al., 1999). Since semaphorin 3A is expressed in r3 and r5, this led to the model that Class 3 semaphorins are secreted from the dorsal midline into the adjacent mesenchyme and form a chemorepulsive barrier that restricts NCCs (Eickholt et al., 1999; Osborne et al., 2005). With this in mind, we expected that functional knockdown of chick neuropilin-1 would result in an inability of cranial NCCs to interpret the semaphorin chemorepulsive signal and invade regions lateral to r3 and r5. Instead, Np-1 siRNA transfected NCCs sorted into and formed stereotypical migratory streams (Figs. 2B and E; Movie 2). A small number of r3 NCCs that aberrantly migrated lateral to r3 reversed direction back towards the neural tube or joined a neighboring migratory stream (data not shown). We confirmed that the Np-1 siRNA construct is produced at initial stages of NCC migration and results in a similar disruption of the r4 migratory pattern (compare Fig. S1-H with Fig. 3B). Our data do not rule out the possibility that other neuropilin–semaphorin interactions are involved in shaping early cranial NCC migratory streams. For example, neuropilin-1 may interact with semaphorin 3A in vivo, but other repulsive cues restrict cranial NCCs transfected with Np-1 siRNA from the regions adjacent to r3 and r5. Alternatively,

neuropilin-2 may play a role in establishing the early NCC migratory stream formation.

Trunk NCCs in neuropilin-2 and semaphorin 3F mutant mice do not follow stereotypical migratory routes and invade typical neural crest cell free zones within the caudal halves of somites (Gammill et al., 2006). Furthermore, when Np-1–Fc/GFP or Np-2–Fc/GFP constructs were electroporated into cranial NCCs, a subpopulation of transfected NCCs were found in the region directly adjacent to r3, but did not migrate out into the distal tissue adjacent to r3 (Osborne et al., 2005). Overexpressing either Np-1–Fc/GFP or Np-2–Fc/GFP in cranial NCC will at least partially perturb semaphorin–neuropilin interactions in general, due to the overlapping binding affinities of neuropilin-1 and neuropilin-2. However, when neuropilin-1 function was knocked down by Np-1 siRNA, any possible neuropilin-2–semaphorin interactions were not affected. Interestingly, the phenotype Osborne et al. (2005) observed was more striking when neuropilin-2 was overexpressed than when neuropilin-1 was overexpressed. This is consistent with the hypothesis that neuropilin-2 is important during the initial migration of r4 cranial NCCs. Finally, in zebrafish *lazarus* mutants, where cranial NCC migration is impaired, neuropilin-2 knockdown rescues a normal NCC migratory pattern (Yu and Moens, 2005). Therefore, semaphorins may cooperate with neuropilin-2 in the initial formation of the r4 NCC migratory streams since *neuropilin-2* is expressed by cranial NCCs (Chilton and Guthrie, 2003; Osborne et al., 2005).

R4 cranial NCCs transfected with Np-1 siRNA displayed significantly fewer filopodia than wildtype NCCs upon reaching the 2nd branchial arch, suggesting a disruption of the NCC cytoskeletal dynamics. The number of NCC filopodia was 31.7% lower in Np-1 siRNA transfected NCCs (Fig. 2H). Time-lapse analyses confirmed that Np-1 siRNA transfected NCCs collapsed filopodia near the entrance to ba2 and stopped (Movie 2). The transfected NCCs did not invade other neighboring regions of the branchial arch. This was surprising since chick trunk NCCs transplanted to permissive regions, but non-NCC migratory pathways are highly motile and invasive (Erickson et al., 1980).

The dramatic change in cell morphologies may be related to NCCs inability to properly sense a branchial arch invasion or distribution signal(s). In other words, there may be unidentified Np-1 ligands present near the entrance and within ba2 that attract r4 cranial NCCs. This phenotype implies that the NCCs fail to sense important extracellular cues and do not properly distribute into the arch. Alternatively, it is possible that the loss of neuropilin signaling may prematurely turn on a NCC stop signal. This would halt the NCCs prior to proper invasion of the branchial arches. Interestingly, when premigratory r4 cranial NCCs were transplanted directly into ba2, Np-1 siRNA transfected cells failed to spread out into the arch, suggesting that Np-1 plays a role in the migration and distribution of NCCs within the arch (Fig. S1-H). When the Np-1 siRNA electroporated embryos were incubated for a longer period of time (36 h), the NCCs failed to recover their cell morphology or properly distribute within the 2nd branchial arch (Fig. 5B). TUNEL staining showed the NCCs did not undergo increased

cell death. Together, our results suggest that NCCs lose their ability to sense an invasion cue when neuropilin-1 function is perturbed.

Subpopulations of r4 cranial NCCs transplanted into mid-r4 host embryos formed narrow, directed migratory streams, suggesting that mid-r4 NCCs do not require contact with local presumptive inhibitory regions lateral to r3 and r5 to reach ba2. The idea of local inhibitory zones adjacent to r3 and r5 to restrict NCC invasion of these regions is a popular hypothesis (Graham et al., 1996; Smith et al., 1997; Farlie et al., 1999; Smith and Graham, 2001; Yu and Moens, 2005). When combined with the hypothesis that population pressure is the driving force of NCC migration (Newgreen et al., 1979; Duband et al., 1985), this would help to explain the formation
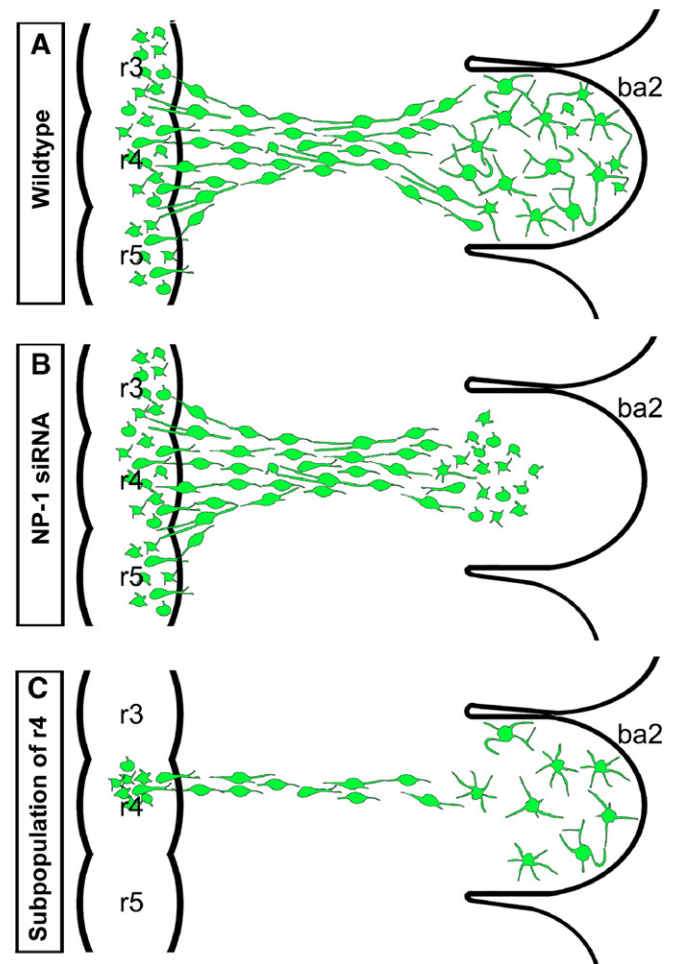

Fig. 7. Schematic model of r4 migratory stream patterning. (A) In wildtype embryos, cranial NCCs from mid-r3 to mid-r5 contribute to the formation of the r4 cranial NCC migratory stream. The cranial NCC are sculpted into a dense stream. Upon arrival to the entrance to ba2, cranial NCCs spread out to invade the entire arch. (B) When neuropilin-1 function was knocked down, a typical r4 cranial NCC migratory stream was formed. However, once the NCCs reach the entrance to ba2, they collapsed filopodia and failed to fully invade the arch. (C) When the population size of r4 cranial NCCs was dramatically reduced, NCCs formed a narrow stream and migrated in a highly directed manner towards ba2 without sampling potential inhibitory zones. Even though the number of NCCs was significantly reduced, they were still able to invade the entire ba2. The notations are r, rhombomere, ba, branchial arch.

of the discrete r4 NCC migratory streams. With this in mind, we expected that by decreasing the number of NCCs and positioning smaller subgroups of transplanted NCCs into the mid-r4 level it would limit the lateral distance the NCCs reached. We also anticipated that transplanted NCC trajectories would resemble a 'pinball' bouncing off of a narrowed, rectangular pool table before reaching the opposite side. Instead, transplanted NCCs formed streams of approximately 1–2 cells wide that migrated the entire length of a typical r4 migratory stream then spread out into ba2 (Fig. 6B; Movie 3). This striking phenotype was observed in host embryos that had undergone ablation as well as embryos that had not, demonstrating that donor cranial NCCs did not tend to mix with endogenous host cranial NCCs during their migration and preferred to migrate with their donor neighbors. Trailing NCCs migrated in a directed manner and maintained neighboring contact with lead cells when analyzed with confocal time-lapse imaging (Movie 3). Surprisingly, the transplanted NCCs did not rely on frequent contact with the environments neighboring r3 or 5 for directional cues (Movie 3). When DiI-labeled r4 NCCs were transplanted into rostral or caudal r4, versus mid-r4, NCCs followed the most directed routes towards ba2, migrating in thin streams (Figs. S1-I–L). Our results support the idea that presumptive inhibitory signals within regions lateral to r3 and r5 act to inhibit invading NCCs (Farlie et al., 1999; Yu and Moens, 2005), but suggest that other signals, possibly attractive factors, may act locally within a corridor lateral to r4 or by cell–cell contact.

We propose a model for cranial NCC migration that includes an in vivo functional role for neuropilin-1 in the invasion of cranial NCC into the branchial arches (Fig. 7). Since we did not see effects to the early NCC stream formation in Np-1 siRNA transfected embryos (Fig. 7B), perhaps other neuropilin–semaphorin or similar repulsive mechanisms prevent aberrant NCC trajectories near the neural tube. Our tissue transplantations combined with confocal time-lapse imaging offered key insights that small subpopulations of NCCs migrated in narrow, directed streams, without sampling presumptive neural crest cell exclusion zones (Fig. 7C). Together, our data support the hypothesis that a combination of permissive, attractive, and inhibitory cues ensures that NCCs reach branchial arch targets in discrete migratory streams (Fig. 7A). We interpret that the failure of NCCs to invade the branchial arches, due to the reduction of neuropilin-1 signaling, was the result of an inability of NCCs to properly sense an invasion signal(s). Further in vivo analysis of molecular interactions assayed by monitoring cell morphology changes and cell migratory behaviors within our system has the potential to reveal the interactions between extracellular signals and intracellular pathways that regulate NCC navigation. The entry of cranial NCCs into the branchial arches is crucial to the development of peripheral structures, including craniofacial components, and necessary for the proper function of the heart and enteric nervous systems. Future in vivo investigations into the role of neuropilin-1 and other related guidance molecules will help to build a molecular framework for cranial NCC migratory patterning.

Appendix A. Supplementary data

Supplementary data associated with this article can be found, in the online version, at doi:10.1016/j.ydbio.2006.08.019.

References

Baker, C.V., Bronner-Fraser, M., 1997. The origins of the neural crest: Part I. embryonic induction. Mech. Dev. 69, 3–11.

Bard, J.B., Hay, E.D., 1975. The behavior of fibroblasts from the developing avian cornea. J. Cell Biol. 67, 400–418.

Birgbauer, E., Sechrist, J., Bronner-Fraser, M., Fraser, S., 1995. Rhombomeric origin and rostrocaudal reassortment of neural crest cells revealed by intravital microscopy. Development 121, 935–945.

Bron, R., Eickholt, B.J., Vermeren, M., Fragale, N., Cohen, J., 2004. Functional knockdown of neuropilin-1 in the developing chick nervous system by siRNA hairpins phenocopies genetic ablation in the mouse. Dev. Dyn. 230, 299–308.

Chilton, J.K., Guthrie, S., 2003. Cranial expression of class 3 secreted semaphorins and their neuropilin receptors. Dev. Dyn. 228, 726–733.

Duband, J.L., Tucker, G.C., Poole, T.J., Vincent, M., Aoyama, H., Thiery, J.P., 1985. How do the migratory and adhesive properties of the neural crest govern ganglia formation in the avian peripheral nervous system? J. Cell Biochem. 27, 189–203.

Eickholt, B.J., Mackenzie, S.L., Graham, A., Walsh, F.S., Doherty, P., 1999. Evidence for collapsin-1 functioning in the control of neural crest migration in both trunk and hindbrain regions. Development 126, 2181–2189.

Erickson, C.A., Tosney, K.W., Weston, J.A., 1980. Analysis of migratory behavior of neural crest and fibroblastic cells in embryonic tissues. Dev. Biol. 77, 142–156.

Farlie, P.G., Kerr, R., Thomas, P., Symes, T., Minichiello, J., Hearn, C.J., Newgreen, D., 1999. A paraxial exclusion zone creates patterned cranial neural crest cell outgrowth adjacent to rhombomeres 3 and 5. Dev. Biol. 213, 70–84.

Farlie, P.G., McKeown, S.J., Newgreen, D.F., 2004. The neural crest: basic biology and clinical relationships in the craniofacial and enteric nervous system. Birth Defects Res. C Embryo. Today 72, 173–189.

Feiner, L., Webber, A.L., Brown, C.B., Lu, M.M., Jia, L., Feinstein, P., Mombaerts, P., Epstein, J.A., Raper, J.A., 2001. Targeted disruption of semaphorin 3C leads to persistent truncus arteriosus and aortic arch interruption. Development 128, 3061–3070.

Fujisawa, H., 2003. Discovery of semaphorin receptors, neuropilin and plexin, and their functions in neural development. J. Neurobiol. 59, 24–33.

Gammill, L.S., Bronner-Fraser, M., 2002. Genomic analysis of neural crest induction. Development 129, 5731–5741.

Gammill, L.S., Gonzalez, C., Gu, C., Bronner-Fraser, M., 2006. Guidance of trunk neural crest migration requires neuropilin 2/semaphorin 3F signaling. Development 133, 99–106.

Gershon, M.D., Ratcliffe, E.M., 2004. Developmental biology of the enteric nervous system: pathogenesis of Hirschsprung's disease and other congenital dysmotilities. Semin. Pediatr. Surg. 13, 224–235.

Golding, J.P., Dixon, M., Gassmann, M., 2002. Cues from neuroepithelium and surface ectoderm maintain neural crest-free regions within cranial mesenchyme of the developing chick. Development 129, 1095–1105.

Golding, J.P., Sobieszczuk, D., Dixon, M., Coles, E., Christiansen, J., Wilkinson, D., Gassmann, M., 2004. Roles of erbB4, rhombomere-specific, and rhombomere-independent cues in maintaining neural crest-free zones in the embryonic head. Dev. Biol. 266, 361–372.

Graham, A., Francis-West, P., Brickell, P., Lumsden, A., 1993. Even-numbered rhombomeres control the apoptotic elimination of neural crest cells from odd-numbered rhombomeres in the chick hindbrain. Development 119, 233–245.

Graham, A., Kontges, G., Lumsden, A., 1996. Neural crest apoptosis and the establishment of craniofacial pattern: an honorable death. Mol. Cell. Neurosci. 8, 76–83.

Graham, A., Begbie, J., McGonnell, I., 2004. Significance of the cranial neural crest. Dev. Dyn. 229, 5–13.

Halloran, M.C., Berndt, J.D., 2003. Current progress in neural crest cell motility and migration and future prospects for the zebrafish model system. Dev. Dyn. 228, 497–513.

Hamburger, V., Hamilton, H.L., 1951. A series of normal stages in the development of the chick embryo. J. Morphol. 88, 49–92.

He, Z., Wang, K.C., Koprivica, V., Ming, G., Song, H., 2002. Knowing how to navigate: mechanisms of semaphorin signaling in the nervous system. Sci. STKE 119, 1–10.

Kawakami, A., Kitsukawa, T., Takagi, S., Fujisawa, H., 1996. Developmentally regulated expression of a cell surface protein neuropilin, in the mouse nervous system. J. Neurobiol. 29, 1–17.

Kontges, G., Lumsden, A., 1996. Rhomboencephalic neural crest segmentation is preserved throughout craniofacial ontogeny. Development 122, 3229–3242.

Kulesa, P.M., Fraser, S.E., 1998. Neural crest cell dynamics revealed by time-lapse video microscopy of whole chick explant cultures. Dev. Biol. 204, 327–344.

Kulesa, P., Bronner-Fraser, M., Fraser, S., 2000. In ovo time-lapse analysis after dorsal neural tube ablation shows rerouting of chick hindbrain neural crest. Development 127, 2843–2852.

Kulesa, P.M., Lu, C.C., Fraser, S.E., 2005. Time-lapse analysis reveals a series of events by which cranial neural crest cells reroute around physical barriers. Brain Behav. Evol. 66, 255–265.

Le Douarin, N.M., Kalcheim, C., 1999. The Neural Crest, 2nd Ed. Cambridge Univ. Press, Cambridge.

Le Douarin, N.M., Creuzet, S., Couly, G., Dupin, E., 2004. Neural crest cell plasticity and its limits. Development 131 (19), 4637–4650.

Lumsden, A., Krumlauf, R., 1996. Patterning the vertebrate neuraxis. Science 274, 1109–1115.

Lumsden, A., Sprawson, N., Graham, A., 1991. Segmental origin and migration of neural crest cells in the hindbrain region of the chick embryo. Development 113, 1281–1291.

Mooney, M.P., Siegel, M.I., 2002. Understanding Craniofacial Anomalies. Wiley-Liss, New York.

Newgreen, D.F., Ritterman, M., Peters, E.A., 1979. Morphology and behaviour of neural crest cells of chick embryo in vitro. Cell Tissue Res. 203, 115–140.

Osborne, N.J., Begbie, J., Chilton, J.K., Schmidt, H., Eickholt, B.J., 2005. Semaphorin/neuropilin signaling influences the positioning of migratory neural crest cells within the hindbrain region of the chick. Dev. Dyn. 232, 939–949.

Schilling, T.F., Kimmel, C.B., 1994. Segment and cell type lineage restrictions during pharyngeal arch development in the zebrafish embryo. Development 120, 483–494.

Sechrist, J., Serbedzija, G.N., Scherson, T., Graser, S.E., Bronner-Fraser, M., 1993. Segmental migration of the hindbrain neural crest does not arise from its segmental generation. Development 118, 691–703.

Sechrist, J., Nieto, M.A., Zamanian, R.T., Bronner-Fraser, M., 1995. Regulative response of the cranial neural tube after neural fold ablation: spatiotemporal nature of neural crest regeneration and up-regulation of Slug. Development 121, 4103–4115.

Smith, A., Graham, A., 2001. Restricting Bmp-4 mediated apoptosis in hindbrain neural crest. Dev. Dyn. 220, 276–283.

Smith, A., Robinson, V., Patel, K., Wilkinson, D.G., 1997. The EphA4 and EphB1 receptor tyrosine kinases and ephrin-B2 ligand regulate targeted migration of branchial neural crest cells. Curr. Biol. 7, 561–570.

Teddy, J.M., Kulesa, P.M., 2004. In vivo evidence for short- and long-range cell communication in cranial neural crest cells. Development 131, 6141–6151.

Tamagnone, L., Comoglio, P.M., 2000. Signalling by semaphorin receptors: cell guidance and beyond. Trends Cell Biol. 10, 377–383.

Trainor, P., Krumlauf, R., 2000. Plasticity in mouse neural crest cells reveals a new patterning role for cranial mesoderm. Nat. Cell Biol. 2, 96–102.

Trainor, P.A., Krumlauf, R., 2001. Hox genes, neural crest cells and branchial arch patterning. Curr. Opin. Cell Biol. 13, 698–705.

Trokovic, N., Trokovic, R., Mai, P., Partanen, J., 2003. Fgfr1 regulates patterning of the pharyngeal region. Genes Dev. 17, 141–153.

Tucker, R.P., Erickson, C.A., 1984. Morphology and behaviour of quail neural crest cells in artificial three-dimensional extracellular matrices. Dev. Biol. 104, 390–405.

Young, H.M., Bergner, A.J., Anderson, R.B., Enomoto, H., Milbrandt, J., Newgreen, D.F., Whitington, P.M., 2004. Dynamics of neural crest-derived cell migration in the embryonic mouse gut. Dev. Biol. 270, 455–473.

Yu, H., Moens, C.B., 2005. Semaphorin signaling guides cranial neural crest cell migration in zebrafish. Dev. Biol. 280, 373–385.